Available online at www.sciencedirect.com
SCIENCE DIRECT®
Journal of Theoretical Biology 232 (2005) 315–328
Journal of Theoretical Biology
www.elsevier.com/locate/yjtbi

Spring-mass running: simple approximate solution and application to gait stability

Hartmut Geyer[a,b,*], Andre Seyfarth[a], Reinhard Blickhan[b]

[a]Locomotion Laboratory, Friedrich–Schiller University Jena, Dornburger Straße 23, 07743 Jena, Germany
[b]Biomechanics Laboratory, Friedrich–Schiller University Jena, Seidelstraße 20, 07749 Jena, Germany

Received 20 February 2004; received in revised form 4 August 2004; accepted 10 August 2004
Available online 27 September 2004

Abstract

The planar spring-mass model is frequently used to describe bouncing gaits (running, hopping, trotting, galloping) in animal and human locomotion and robotics. Although this model represents a rather simple mechanical system, an analytical solution predicting the center of mass trajectory during stance remains open. We derive an approximate solution in elementary functions assuming a small angular sweep and a small spring compression during stance. The predictive power and quality of this solution is investigated for model parameters relevant to human locomotion. The analysis shows that (i), for spring compressions of up to 20% (angle of attack $\geqslant 60^\circ$, angular sweep $\leqslant 60^\circ$) the approximate solution describes the stance dynamics of the center of mass within a 1% tolerance of spring compression and 0.6° tolerance of angular motion compared to numerical calculations, and (ii), despite its relative simplicity, the approximate solution accurately predicts stable locomotion well extending into the physiologically reasonable parameter domain. (iii) Furthermore, in a particular case, an explicit parametric dependency required for gait stability can be revealed extending an earlier, empirically found relationship. It is suggested that this approximation of the planar spring-mass dynamics may serve as an analytical tool for application in robotics and further research on legged locomotion.

Keywords: Biomechanics; Spring mass running; Stability; Approximate solution

1. Introduction

The astonishing elegance and efficiency with which legged animals and humans traverse natural terrain outclasses any present day man-made competitor. Beyond sheer fascination, such a 'technological' superiority heavily attracts the interest from many scientists. Yet it seems that, despite intensive research activities in fields as diverse as biomechanics, robotics, and medicine, the overwhelming complexity in biological systems may deny a comprehensive understanding of all the functional details of their legged locomotor apparatus. Considering this, in some studies complex integral representations are discarded in favor of simpler models seeking least parameter descriptions of aspects of the problem at hand. Without claiming to capture the whole system, these models may well be suited to succeed in identifying some underlying principles of pedal locomotion.

In particular, on the mechanical level, the planar spring-mass model for bouncing gaits (Blickhan, 1989; McMahon and Cheng, 1990) has drawn attention since, while advocating a largely reductionist description, it retains key features discriminating legged from wheeled systems: phase switches between flight (swing) and stance phase, a leg orientation, and a repulsive leg behavior in stance. In consequence, not only biomechanical studies investigating hopping (Farley et al., 1991; Seyfarth et al., 2001) or running (He et al., 1991; Farley et al., 1993), but also fast legged robots driven by model-based control

*Corresponding author. Locomotion Laboratory, Friedrich–Schiller University Jena, Dornburger Straße 23, 07743 Jena, Germany. Tel.: +49-3641-945733; fax: +49-3641-945732.
E-mail address: hartmut.geyer@uni-jena.de (H. Geyer).

0022-5193/$ - see front matter © 2004 Elsevier Ltd. All rights reserved.
doi:10.1016/j.jtbi.2004.08.015

algorithms (Raibert, 1986; Saranli and Koditschek, 2003) rely on this plant. Yet still, even for the simple spring-mass model, parametric insights remain obscured as the dynamics of the stance phase are non-integrable (Whittacker, 1904). Lacking a closed form solution, research is either bound to extensive numerical investigations or needs to establish suitable approximations.

For instance, by mapping the model's parameter space, simulation studies suggest that the spring-mass system for running can display a 'self-stable' behavior (Seyfarth et al., 2002; Ghigliazza et al., 2003). Here, self-stability refers to the observation of asymptotically stable gait trajectories without continuous sensory feedback. As the spring-mass model is energy preserving, i.e. non-dissipative, this behavior seems counter-intuitive. However, it also constitutes a piecewise holonomic system experiencing phase-dependent dynamics (the different stance and flight-phase dynamics), and several recent investigations demonstrate that such systems can exhibit asymptotic stability (Coleman et al., 1997; Ruina, 1998; Coleman and Holmes, 1999).

Analytical investigations assessing this issue for the spring-mass model in particular, for reasons of accessibility, mostly neglect gravity when approximating the stance-phase dynamics (e.g. Ghigliazza et al., 2003). As this can hardly be done in general locomotion (Schwind and Koditschek, 2000) or when addressing physiologically motivated parameters (Geyer, 2001), in Schwind and Koditschek (2000) an iterative algorithm reincorporating the effect of gravity is introduced. Although the quality of the approximate solution improves with each iteration, its decreasing mathematical tractability hampers the intended deeper parametric insight into the functional relations.

In this study, a comparably simple approximate solution for the dynamics of the planar spring-mass model is derived including gravitational effects. Within the scope of stability in spring-mass running, the predictive power and the quality of this solution are investigated. The former by considering a special case, the latter by comparing a return-map analysis based on the approximation with numerical results throughout the range of the parameters spring stiffness, angle of attack, and system energy. In both situations, model parameters relevant to human locomotion are addressed.

2. Spring-mass running

2.1. Model

Planar spring-mass running is characterized by alternating flight and contact phases. As described previously (Seyfarth et al., 2002), during flight the center of mass trajectory is influenced by the gravitational force. Here, a virtual leg of length ℓ_0 and a constant angle of attack

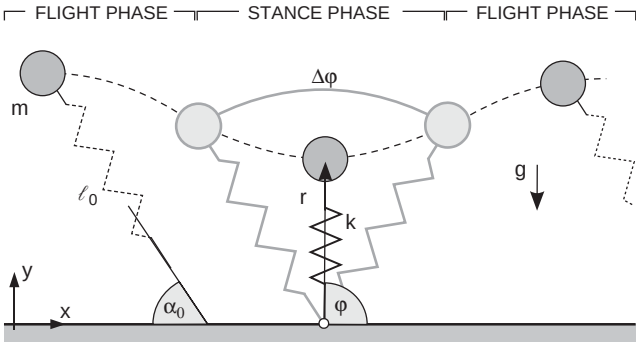

Fig. 1. Spring-mass model for running. Parameters: m—point mass, ℓ_0— rest length, α_0—leg angle of attack during flight, g—gravitational acceleration, k—spring stiffness, r—radial and φ—angular position of the point mass, $\Delta\varphi$—angle swept during stance.

α_0 are assumed (Fig. 1). When the leg strikes the ground, the dynamic behavior of spring-mass running is further influenced by the force exerted by the leg spring (stiffness k, rest length ℓ_0) attached to the center of mass. The transition from stance-to-flight occurs if the spring reaches its rest length again during lengthening.

2.2. Apex return map

To investigate periodicity for this running model, it suffices to consider the apex height y_i of two subsequent flight phases. This holds since (i) at apex the vertical velocity $\dot{y}_i$ equals zero, (ii) the forward velocity $\dot{x}_i$ can be expressed in terms of the apex height due to the constant system energy E_s, and (iii) the forward position x_i has no influence on the further system dynamics.

Consequently, the stability of spring-mass running can be analysed with a one-dimensional return map $y_{i+1}(y_i)$ of the apex height of two subsequent flight phases (single-step analysis). In terms of the apex return map, a periodic movement trajectory in spring-mass running is represented by a fixed point $y_{i+1}(y_i) = y_i$. Moreover, as a sufficient condition, a slope $\mathrm{d}y_{i+1}(y_i)/\mathrm{d}y_i$ within a range of $(-1, 1)$ in the neighborhood of the fixed point indicates the stability of the movement pattern (higher than period 1 stability, which corresponds to symmetric contacts with time reflection symmetry about midstance, is not considered). The size of the neighborhood defines the basin of attraction of the stable trajectory.

3. Approximate solution

3.1. Model approximations

The analytical solution for the center of mass motion during flight is well known (ballistic flight trajectory), but a different situation applies to the stance phase. Using polar coordinates (r, φ), the Lagrange function of

the contact phase is given by (see Fig. 1 for notation)

$$L = \frac{m}{2}(\dot{r}^2 + r^2\dot{\varphi}^2) - \frac{k}{2}(\ell_0 - r)^2 - mgr\sin\varphi. \quad (1)$$

From the Lagrange function, the derived center of mass dynamics are characterized by a set of coupled nonlinear differential equations. As of today, the analytical solution for the contact phase remains open. For such situations, a common approach is to ask for simplifications, which could provide an approximate solution. In the case of Eq. (1), for sufficiently small angles $\Delta\varphi$ swept during stance, the sine term on the right-hand side can assumed to be

$$\sin\varphi \approx 1 \quad (2)$$

and the equations of motion simplify to

$$m\ddot{r} = k(\ell_0 - r) + mr\dot{\varphi}^2 - mg \quad (3)$$

and

$$\frac{\mathrm{d}}{\mathrm{d}t}(mr^2\dot{\varphi}) = 0 \quad (4)$$

transforming the spring-mass model into an integrable central force system, where the mechanical energy E and the angular momentum $P = mr^2\dot{\varphi}$ are conserved.

To derive the apex return map $y_{i+1}(y_i)$, it suffices to identify the system state at the phase transitions (flight-to-stance and stance-to-flight), regardless of the actual motion during stance. Due to both, the radial symmetry of the model (spring assumes rest length ℓ_0 at each phase transition) and the conservation of angular momentum (4), the system state at take-off (TO) relates to the state at touch-down (TD) with

$$\begin{aligned} r_{TO} &= r_{TD}, \\ \dot{r}_{TO} &= -\dot{r}_{TD}, \\ \varphi_{TO} &= \varphi_{TD} + \Delta\varphi, \\ \dot{\varphi}_{TO} &= \dot{\varphi}_{TD}, \end{aligned} \quad (5)$$

where only the angle $\Delta\varphi$ swept during stance cannot simply be expressed by the state at touch-down. Hence, we will calculate this angle from the dynamics of the central force system (3) and (4) in the following sections. Particularly, we will first derive the radial motion $r(t)$ and then integrate $\dot{\varphi} = \frac{P}{mr^2}$. In both cases, we will use the further assumption of small relative spring amplitudes

$$|\rho| \ll 1 \quad (6)$$

with $\rho = \frac{r-\ell_0}{\ell_0} \leqslant 0$ to attain an approximate solution of the central force system and, consequently, of the planar spring-mass dynamics in elementary functions.

3.2. Radial motion during stance

Using the conservation of angular momentum P, the constant mechanical energy of the contact phase is given by

$$E = \frac{m}{2}\dot{r}^2 + \frac{P^2}{2mr^2} + \frac{k}{2}(\ell_0 - r)^2 + mgr. \quad (7)$$

Applying the substitutions $\varepsilon = \frac{2E}{m\ell_0^2}$, $\omega = \frac{P}{m\ell_0^2}$, and $\omega_0 = \sqrt{\frac{k}{m}}$, the equation rewrites to

$$\varepsilon = \dot{\rho}^2 + \frac{\omega^2}{(1+\rho)^2} + \omega_0^2\rho^2 + \frac{2g}{\ell_0}(1+\rho), \quad (8)$$

where ρ represents the relative spring amplitude introduced in the previous section. The term $\frac{1}{(1+\rho)^2}$ can be represented as a Taylor expansion around the initial relative amplitude $\rho = 0$

$$\left.\frac{1}{(1+\rho)^2}\right|_{\rho=0} = 1 - 2\rho + 3\rho^2 - O(\rho^3). \quad (9)$$

The restriction (6) to small values of ρ allows to truncate the expansion after the square term. Hence, the differential equation (8) transforms into

$$t = \int \frac{\mathrm{d}\rho}{\sqrt{\lambda\rho^2 + \mu\rho + \nu}}, \quad (10)$$

where the factors are given by $\lambda = -(3\omega^2 + \omega_0^2)$, $\mu = 2(\omega^2 - g/\ell_0)$, and $\nu = (\varepsilon - \omega^2 - 2g/\ell_0)$. The integral in Eq. (10) is given by

$$\int \frac{\mathrm{d}\rho}{\sqrt{\lambda\rho^2 + \mu\rho + \nu}} = -\frac{1}{\sqrt{-\lambda}} \times \arcsin\left(\frac{2\lambda\rho + \mu}{\sqrt{\mu^2 - 4\lambda\nu}}\right), \quad (11)$$

provided that both the factor λ and the expression $4\lambda\nu - \mu^2$ are negative. The first condition is fulfilled by the definition of λ. The second one holds if ν is positive. Since ν is constant, it suffices to check this condition at the instant of touch-down. From here it follows that $\nu = \dot{r}_0^2/\ell_0^2$. Using Eq. (11), Eq. (10) can be resolved and yields the general radial motion

$$r(t) = \ell_0(1 + a + b\sin\hat{\omega}_0 t) \quad (12)$$

with

$$\begin{aligned} a &= \frac{\omega^2 - g/\ell_0}{\omega_0^2 + 3\omega^2}, \\ b &= \frac{\sqrt{(\omega^2 - g/\ell_0)^2 + (\omega_0^2 + 3\omega^2)(\varepsilon - \omega^2 - 2g/\ell_0)}}{\omega_0^2 + 3\omega^2}, \\ \hat{\omega}_0 &= \sqrt{\omega_0^2 + 3\omega^2}. \end{aligned}$$

The radial motion $r(t)$ describes a harmonic oscillation around the length $\ell_0(1+a)$ with an amplitude $\ell_0 b$ and an angular frequency $\hat{\omega}_0$ (Fig. 2). However, the solution $r(t)$ only holds for the contact phase of spring-mass running where $r \leqslant \ell_0$. Using the condition $r = \ell_0$,

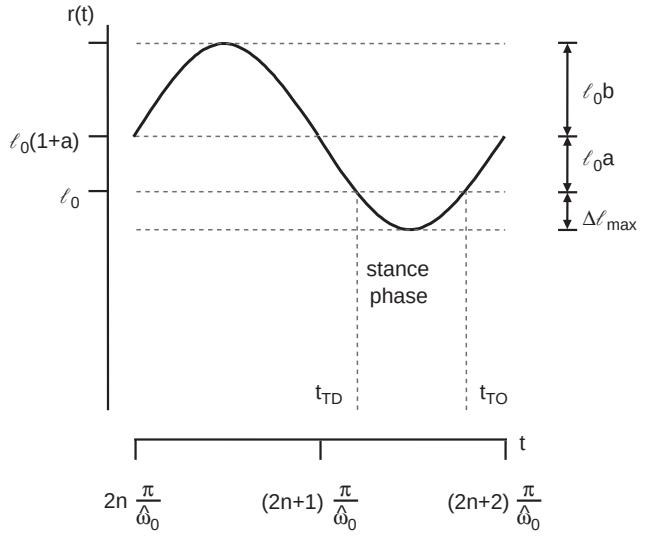

Fig. 2. General solution for the radial motion $r(t)$ during stance describing a sinusoidal oscillation around $r = \ell_0(1 + a)$ with amplitude $\ell_0 b$ and frequency $\hat{\omega}_0$. The solution only holds for $r(t) \leqslant \ell_0$. Note that a can also be negative shifting ℓ_0 above $\ell_0(1 + a)$. $\Delta\ell_{max}$— maximum leg compression.

Eq. (12) can be resolved to identify the instances of touch-down and take-off (Fig. 2)

$$t_{TD} = \frac{1}{\hat{\omega}_0}\left\{\left(2n + \frac{3}{2}\right)\pi - \left[\frac{\pi}{2} + \arcsin\left(-\frac{a}{b}\right)\right]\right\} \tag{13}$$

and

$$t_{TO} = \frac{1}{\hat{\omega}_0}\left\{\left(2n + \frac{3}{2}\right)\pi + \left[\frac{\pi}{2} + \arcsin\left(-\frac{a}{b}\right)\right]\right\} \tag{14}$$

where n is an arbitrary integer.

The maximum spring compression $\Delta\ell_{max}$ during stance is given by the difference of the amplitude $\ell_0 b$ of $r(t)$ and the shift $\ell_0 a$ of the touch-down position $r(t_{TD}) = \ell_0$ (Fig. 2). Thus, restriction (6) to small values of ρ is adequately formulated by

$$b - a \ll 1. \tag{15}$$

3.3. Angle swept during stance

With the radial motion $r(t)$, the angle swept during stance can be derived from the equation $P = mr^2\dot{\varphi}$ describing the constant angular momentum. Using the substitutions ω and ρ, the angular velocity is given by

$$\dot{\varphi} = \frac{\omega}{(1 + \rho)^2}. \tag{16}$$

To integrate Eq. (16), again, we use the Taylor expansion (9), but cancel this expansion after the linear term already. The Taylor expansion of $\frac{1}{(1+\rho)^2}$ to the second order in ρ for both the r- and φ-trajectory would lead to a more accurate approximate solution of the central force dynamics (3) and (4). However, approximating the actual spring-mass dynamics (1), the central force approach (2) is error-prone itself. Carrying out the expansion to the first-order only for $\dot{\varphi}$ allows in part to compensate for the error introduced by this general approach (see appendix).

With $\dot{\varphi} = \omega(1 - 2\rho)$ and substituting ρ by r, we obtain the angle $\Delta\varphi$ swept during stance

$$\Delta\varphi = \int_{t_{TD}}^{t_{TO}} \omega[(1 - 2a) - 2b \sin\hat{\omega}_0 t]\,\mathrm{d}t. \tag{17}$$

Considering Eqs. (13) and (14) as integration limits, and using the identities $\cos(\arcsin x) = \sqrt{1 - x^2}$ and $\pi + 2\arcsin\left(-\frac{a}{b}\right) = 2\arccos\left(\frac{a}{b}\right)$, the angle swept during stance resolves to

$$\Delta\varphi = 2\frac{\omega}{\hat{\omega}_0}\left[(1 - 2a)\arccos\frac{a}{b} + 2\sqrt{b^2 - a^2}\right]. \tag{18}$$

As both the mechanical energy and the angular momentum are conserved, the parameters ω, $\hat{\omega}_0$, a and b can be related to the system state at touch-down by solving Eqs. (4) and (8) at this instant. Therefore, $\Delta\varphi$ is uniquely determined by the system state at touch-down (ℓ_0, $\dot{r}_{TD}$, φ_{TD}, $\dot{\varphi}_{TD}$) and the parameters of the spring-mass system (k, m, g). Although not explicitly appearing when re-substituting in Eq. (18), the landing angle $\varphi_{TD} = \pi - \alpha_0$ influences $\Delta\varphi$ by determining the distribution of the landing velocity to the radial and angular component.

3.4. Approximate solution

By defining the instant of touch-down as $t = 0$, the radial (12) and angular motions during stance (17) rewrite to

$$r(t) = \ell_0 + \ell_0[a(1 - \cos\hat{\omega}_0 t) - \sqrt{b^2 - a^2}\sin\hat{\omega}_0 t], \tag{19}$$

$$\varphi(t) = \varphi_{TD} + (1 - 2a)\omega t + \frac{2\omega}{\hat{\omega}_0} \times[a\sin\hat{\omega}_0 t + \sqrt{b^2 - a^2}(1 - \cos\hat{\omega}_0 t)] \tag{20}$$

with t ranging from 0 to $t_c = [\pi + 2\arcsin(-a/b)]/\hat{\omega}_0$. By substituting a and b (12) as well as expressing ε, ω, and ω_0 with the system state at touch-down, the center of mass trajectory during stance resolves to

$$r(t) = \ell_0 - \frac{|\dot{r}_{TD}|}{\hat{\omega}_0}\sin\hat{\omega}_0 t + \frac{\dot{\varphi}_{TD}^2\ell_0 - g}{\hat{\omega}_0^2}(1 - \cos\hat{\omega}_0 t), \tag{21}$$

$$\varphi(t) = \pi - \alpha_0 + \left(1 - 2\frac{\dot{\varphi}_{TD}^2 - g/\ell_0}{\hat{\omega}_0^2}\right)\dot{\varphi}_{TD}t + \frac{2\dot{\varphi}_{TD}}{\hat{\omega}_0}\left[\frac{\dot{\varphi}_{TD}^2 - g/\ell_0}{\hat{\omega}_0^2}\sin\,\hat{\omega}_0 t + \frac{|\dot{r}_{TD}|}{\hat{\omega}_0\ell_0}(1 - \cos\,\hat{\omega}_0 t)\right]. \quad (22)$$

The radial motion corresponds to the motion of a one-dimensional spring-mass system under the influence of gravity except for the increased oscillation frequency $\hat{\omega}_0 = \sqrt{k/m + 3\dot{\varphi}_{TD}^2}$. The angular motion has a linear characteristic, which is modulated by trigonometric functions. The time in contact resolves to

$$t_c = \frac{1}{\hat{\omega}_0}\left[\pi + 2\arctan\left(\frac{g - \ell_0\dot{\varphi}_{TD}^2}{|\dot{r}_{TD}|\hat{\omega}_0}\right)\right]. \quad (23)$$

4. Stability of spring-mass running

4.1. Analytical apex return map

In the following section we use the derived analytical solution for the contact to calculate the dependency of two subsequent apex heights. Based on this apex return map, for a special case, we derive an explicit parametric dependency required for stable spring-mass running and, within the scope of gait stability, compare parameter predictions with previous numerical results.

With the angle swept during stance (18), we know how the system state at take-off relates to the initial state of the contact phase at touch-down (5). But, to apply the correct initial values, the mapping between the apex height y_i and the touch-down state in polar coordinates is required

$$y_i \mapsto \begin{bmatrix} \dot{x} = \sqrt{\frac{2}{m}(E_s - mgy_i)} \\ y = \ell_0\,\sin\,\alpha_0 \\ \dot{y} = -\sqrt{2g(y_i - y)} \end{bmatrix}_{TD} \mapsto \begin{bmatrix} r = \ell_0 \\ \dot{r} = \dot{x}\cos\,\varphi + \dot{y}\,\sin\,\varphi \\ \varphi = \pi - \alpha_0 \\ \dot{\varphi} = \frac{1}{\ell_0}(\dot{y}\cos\,\varphi - \dot{x}\,\sin\,\varphi) \end{bmatrix}_{TD}, \quad (24)$$

where E_s is the system energy prior to touch-down (for details see Sections 2.2 and 4.2). To obtain the apex return map $y_{i+1}(y_i)$, the system state at the following apex $i+1$ has to be derived, i.e. the mapping between the state at take-off and the apex $i+1$ is further required

$$\begin{bmatrix} \dot{x} = \dot{r}\cos\,\varphi - \ell_0\dot{\varphi}\,\sin\,\varphi \\ y = \ell_0\,\sin\,\varphi \\ \dot{y} = \dot{r}\,\sin\,\varphi + \ell_0\dot{\varphi}\cos\,\varphi \end{bmatrix}_{TO} \mapsto \begin{bmatrix} \dot{x}_{i+1} = \dot{x}_{TO}, \\ y_{i+1} = y_{TO} + \frac{1}{2g}\dot{y}_{TO} \end{bmatrix}. \quad (25)$$

Using both mappings, the apex return map function of approximated spring-mass running can be constructed and yields after simplification

$$y_{i+1}(y_i) = \frac{1}{mg}\left[\cos(\Delta\varphi - 2\alpha_0)\sqrt{mg(y_i - \ell_0\sin\,\alpha_0)} + \sin(\Delta\varphi - 2\alpha_0)\sqrt{E_s - mgy_i}\right]^2 + \ell_0\,\sin(\alpha_0 - \Delta\varphi). \quad (26)$$

Next to the preceding apex height (y_i), y_{i+1} is a function of the system energy (E_s), the landing leg configuration (ℓ_0, α_0), and the dynamic response of the spring-mass system (k, m, g). However, the apex return map can only exist where y_{i+1} exceeds the landing height $y_{i+1} \geqslant \ell_0\,\sin\,\alpha_0$. Otherwise, the leg would extend into the ground (stumbling).

4.2. System energy correction

For spring-mass running, the stability analysis can be performed based on a one-dimensional apex return map since the system energy E_s remains constant (see Section 2.2). When using the approximation for the stance phase, in particular due to assumption (2), this conservation of energy is violated if the vertical position at take-off differs from that at touch-down ($y_{TD} \neq y_{TO}$, i.e. asymmetric contact phase):

In a central force system approach, the kinetic energy $\frac{m}{2}(\dot{r}^2 + r^2\dot{\varphi}^2)$ is equal at touch-down and take-off (5), regardless of the angle swept during stance. At the transitions between flight and stance phase the direction of the gravitational force 'switches' between vertical and leg orientation. The corresponding shifts in energy at touch-down and take-off compensate each other for symmetric stance phases ($y_{TD} = y_{TO}$). In contrast, for asymmetric contact phases, a net change in system energy $\Delta E = mg(y_{TO} - y_{TD})$ occurs. To restore the conservative nature of the model ($E_s = const$), this change is corrected in (25) by readjusting the horizontal velocity to

$$\dot{x}_{i+1} = \sqrt{\frac{2}{m}(E_s - mgy_{i+1})}. \quad (27)$$

When reapplying the apex return map (26) for the new apex height y_{i+1}, this is automatically taken into account by reusing the system energy E_s.

4.3. Stability analysis: the special case $a = 0$

From Eq. (26) we obtain that the fixed point condition $y_{i+1}(y_i) = y_i$ is fulfilled if Eq. (18) describes symmetric contacts with $\Delta\varphi = 2\alpha_0 - \pi$. In general, solving Eq. (18) appears to be difficult since this equation involves nonlinearities. However, in order to demonstrate the existence and stability of fixed points of the apex return map, it suffices to present one example. In the following, we will confine our investigation to the special case $a = 0$, i.e. when the angular velocity at touch-down is identical to the pendulum frequency $\omega = \dot{\varphi}_{TD} = -\sqrt{g/\ell_0}$ (although $\omega = +\sqrt{g/\ell_0}$ equally satisfies $a = 0$, we are concerned with forward locomotion only). In this particular situation, Eq. (18) considerably simplifies to

$$\Delta\varphi(\tilde{k}, \alpha_0, \tilde{E}_s) = -\frac{2}{\sqrt{\tilde{k}+3}} \times \left(\frac{\pi}{2} + 2\sqrt{\frac{2\tilde{E}_s - 1 - 2\sin\alpha_0}{\tilde{k}+3}}\right) \tag{28}$$

where $\tilde{k} = \frac{k\ell_0}{mg}$ represents the dimensionless spring stiffness and $\tilde{E}_s = \frac{E_s}{mg\ell_0}$ is the dimensionless system energy.[1]

Apart from its mathematical simplicity, this special case addresses a characteristic running speed in animals and humans. Considering that, for rather steep angles of attack, the horizontal velocity $\dot{x}$ relates to the angular velocity with $\dot{x} \approx \ell_0\dot{\varphi}_{TD}$, the case $a = 0$ describes running with a Froude number $Fr = \frac{\dot{x}^2}{g\ell_0} = 1$, which is close to the preferred trotting speed in horses (Alexander, 1989; Wickler et al., 2001) or to a typical jogging speed in humans (Alexander, 1989).

4.3.1. Existence of fixed points

Before continuing with Eq. (28), we need to check whether apex states y_i restricted by the touch-down condition $\omega = -\sqrt{g/\ell_0}$ can be found. By using the apex-to-touch-down map (24), we find the formal expression

$$\omega = \sqrt{\frac{2g}{\ell_0}}\left(\cos\alpha_0\sqrt{y_i/\ell_0 - \sin\alpha_0} - \sin\alpha_0\sqrt{\tilde{E}_s - y_i/\ell_0}\right). \tag{29}$$

Resolving for $\omega = -\sqrt{g/\ell_0}$ leads to the corresponding apex height

$$\begin{aligned} y_i &= \ell_0\sin\alpha_0 + \frac{\ell_0}{2}\left(\cos\alpha_0 - \sin\alpha_0\sqrt{2\tilde{E}_s - 1 - 2\sin\alpha_0}\right)^2 \\ &= \ell_0\tilde{E}_s - \frac{\ell_0}{2}\left(\sin\alpha_0 + \cos\alpha_0\sqrt{2\tilde{E}_s - 1 - 2\sin\alpha_0}\right)^2. \end{aligned} \tag{30}$$

However, substituting (30) back into (29) yields

$$\begin{aligned} -1 = \cos\alpha_0&\left|\cos\alpha_0 - \sin\alpha_0\sqrt{2\tilde{E}_s - 1 - 2\sin\alpha_0}\right| \\ &- \sin\alpha_0\left|\sin\alpha_0 + \cos\alpha_0\sqrt{2\tilde{E}_s - 1 - 2\sin\alpha_0}\right| \end{aligned} \tag{31}$$

and it follows that the solution (30) only holds if $\cos\alpha_0 \leqslant \sin\alpha_0\sqrt{2\tilde{E}_s - 1 - 2\sin\alpha_0}$, i.e. the system energy fulfils $\tilde{E}_s \geqslant \tilde{E}_s^{\min}$ with

$$\tilde{E}_s^{\min} = \frac{1}{2\sin^2\alpha_0} + \sin\alpha_0. \tag{32}$$

For a system energy $\tilde{E}_s = \tilde{E}_s^{\min}$, the apex height is identical to the landing height $y_i = \ell_0\sin\alpha_0$. Above this level $\tilde{E}_s > \tilde{E}_s^{\min}$, the apex height increases, but never approaches the upper boundary $y_i = \ell_0\tilde{E}_s$.

Having established the flight-phase limitations for the existence of apex states y_i characterized by $a = 0$, we can proceed with Eq. (28). Solving for $\Delta\varphi = 2\alpha_0 - \pi$ involves a quadratic equation for $\sqrt{\tilde{k}+3}$, which has only one physically reasonable solution yielding an expression for the required spring stiffness

$$\tilde{k}(\alpha_0, \tilde{E}_s) = \frac{\left[\pi + \sqrt{\pi^2 + 32\left(\frac{\pi}{2} - \alpha_0\right)\sqrt{2\tilde{E}_s - 1 - 2\sin\alpha_0}}\right]^2}{16\left(\frac{\pi}{2} - \alpha_0\right)^2} - 3. \tag{33}$$

At given angle of attack ($\alpha_0 \in \left[0, \frac{\pi}{2}\right]$ in forward locomotion), the stiffness is lowest for the minimum system energy

$$\tilde{k}^{\min}(\alpha_0) = \tilde{k}^{\min}(\alpha_0, \tilde{E}_s^{\min}) = \frac{\left[\pi + \sqrt{\pi^2 + 32\left(\frac{\pi}{2} - \alpha_0\right)\frac{\cos\alpha_0}{\sin\alpha_0}}\right]^2}{16\left(\frac{\pi}{2} - \alpha_0\right)^2} - 3 \tag{34}$$

with increasing system energy $\tilde{E}_s > \tilde{E}_s^{\min}$, a larger spring stiffness is required to ensure symmetric contacts (Fig. 3).

[1] The appearance of $\tilde{k}$ and $\tilde{E}_s$ is not restricted to the special case $a = 0$. Rather, these substitutes can be identified as independent parameter groups when applying a dimensional analysis of the governing equations in spring-mass running. Specifically, the dimensionless stiffness $\tilde{k}$ is a well-known parameter group frequently used in comparative studies on animal and human locomotion (e.g. Blickhan, 1989; Blickhan and Full, 1993).

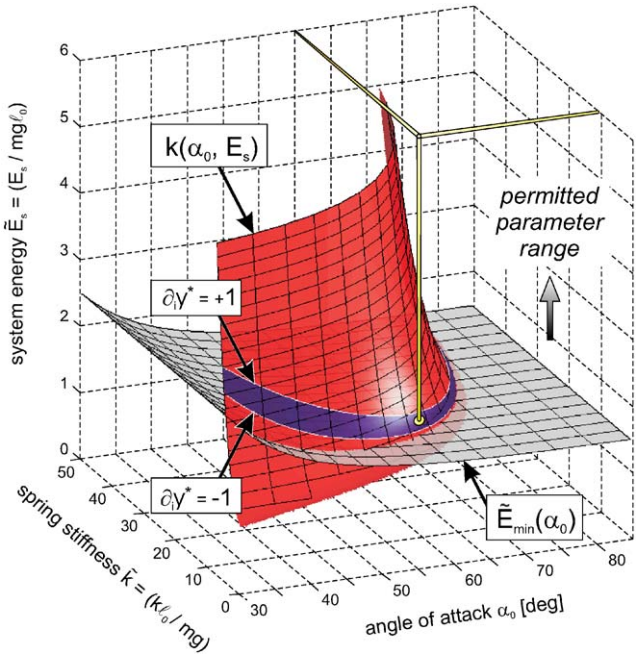

Fig. 3. Parameter interdependence for fixed point solutions with $a = 0$. The fixed points can only exist if a minimum energy $\tilde{E}_{\min}(\alpha_0)$ is exceeded (permitted parameter range). Above this level, the required parameter combinations of angle of attack α_0, system energy $\tilde{E}_s$, and spring stiffness $\tilde{k}$ are defined by relation (33) describing a sub set $\tilde{k}(\alpha_0, \tilde{E}_s)$ within the parameter space. The dark area within this sub set characterizes stable fixed point solutions (see Section 4.3.2). The open lines indicate the parameter combination that is used as apex return map example in Fig. 4.

With Eqs. (32) and (33) we have identified the parameter dependence required for periodic locomotion constrained by $\omega = -\sqrt{g/\ell_0}$. Although the resulting steady-state solutions (30) demonstrate the existence of fixed points of the apex return map, it remains to investigate to what extent the derived parameter relations represent stable gait patterns.

4.3.2. Stability of fixed points

Stable fixed point solutions y_i are characterized by

$$-1 < \frac{\partial}{\partial y_i}[y_{i+1}(y_i)]_{y_{i+1}=y_i} = \partial_i y^* < 1. \tag{35}$$

To prove stability, we need to identify at least one parameter set $(\alpha_0, \tilde{E}_s)$ leading to solutions y_i satisfying Eq. (35). Starting with Eq. (26), we obtain

$$\partial_i y^* = 1 + \left[\ell_0 \cos\alpha_0 + 2\sqrt{(\ell_0\tilde{E}_s - y_i)(y_i - \ell_0 \sin\alpha_0)}\right]\partial_i\Delta\varphi^* \tag{36}$$

by using $\Delta\varphi = 2\alpha_0 - \pi$ for symmetric contacts. As the bracketed expression always remains positive, Eq. (35) transforms into a condition for the angle swept during stance $\partial_i\Delta\varphi^* \in \left(-\frac{2}{\ell_0\cos\alpha_0 + 2\sqrt{(\ell_0\tilde{E}_s - y_i)(y_i - \ell_0\sin\alpha_0)}}, 0\right)$ indicating that disturbed apex conditions towards higher (lower) apices must be compensated for by a larger (smaller) amount of angular sweep in contact ($\Delta\varphi^*$ is negative). However, to remain stable, the rate of this 'negative' correlation must not exceed $-\frac{2}{\ell_0\cos\alpha_0 + 2\sqrt{(\ell_0\tilde{E}_s - y_i)(y_i - \ell_0\sin\alpha_0)}}$. From Eq. (18) it follows that

$$\partial_i\Delta\varphi^* = \left(\frac{1}{\omega} - \frac{3\omega}{\hat{\omega}_0^2}\right)(2\alpha_0 - \pi)\partial_i\omega^* - 2\frac{\omega}{\hat{\omega}_0}\left[2\arccos\left(\frac{a}{b}\right)\partial_i a^* - \frac{\left(\frac{a}{b} - 2\frac{a^2}{b} + 2b\right)\partial_i b^* - \partial_i a^*}{\sqrt{b^2 - a^2}}\right], \tag{37}$$

which, by expressing $\partial_i a^*$ and $\partial_i b^*$ with $\partial_i\omega^*$, and resolving $\partial_i\omega^*$, can be further deduced to

$$\partial_i\Delta\varphi^* = \left\{\left(\frac{1}{\omega} - \frac{3\omega}{\hat{\omega}_0^2}\right)(2\alpha_0 - \pi) - 2\frac{\omega^2}{\hat{\omega}_0^3} \times \left[(4 - 12a)\arccos\left(\frac{a}{b}\right) - \frac{\left(\frac{a}{b} - 2\frac{a^2}{b} + 2b\right)\left(2\frac{a}{b} - \frac{1}{b} - 3\frac{a^2}{b} - 3b\right) - 2 + 6a}{\sqrt{b^2 - a^2}}\right]\right\} \times \frac{\sqrt{2g}}{2\ell_0}\left(\frac{\cos\alpha_0}{\sqrt{y_i^* - \ell_0\sin\alpha_0}} + \frac{\sin\alpha_0}{\sqrt{\ell_0\tilde{E}_s - y_i^*}}\right). \tag{38}$$

Note that Eq. (38) is valid for any fixed point solution with symmetric contacts $\Delta\varphi^* = 2\alpha_0 - \pi$ since $a = 0$ has not yet been utilized. Finally, applying $a = 0$ and $\omega = -\sqrt{g/\ell_0}$ yields

$$\partial_i\Delta\varphi^* = \frac{1}{\tilde{k} + 3}\left[\tilde{k}\left(\frac{\pi}{2} - \alpha_0\right) - \frac{2\pi}{\sqrt{\tilde{k} + 3}} - \frac{6\sqrt{2\tilde{E}_s - 1 - 2\sin\alpha_0}}{\tilde{k} + 3} - \frac{4}{\sqrt{2\tilde{E}_s - 1 - 2\sin\alpha_0}}\right] \times \sqrt{\frac{2}{\ell_0}}\left(\frac{\cos\alpha_0}{\sqrt{y_i^* - \ell_0\sin\alpha_0}} + \frac{\sin\alpha_0}{\sqrt{\ell_0\tilde{E}_s - y_i^*}}\right). \tag{39}$$

By substituting Eq. (39) back into Eq. (36) and using Eq. (30) as well as Eq. (33), we obtain an expression $\partial_i y^* = \partial_i y^*(\alpha_0, \tilde{E}_s)$ identifying the parameter dependence

of the derivative of the apex height return map $y_{i+1}(y_i)$ at the fixed points y_i^* in the special case $a = 0$.

Based on this result, in Fig. 3, parameter combinations leading to stable fixed points are indicated in the $\tilde{k}(\alpha_0, \tilde{E}_s)$–region as dark area, which is limited by two curves denoting the lower ($\partial_i y^* = -1$) and upper constraint ($\partial_i y^* = +1$) for stable solutions (35). Although this area narrows and almost diminishes below the minimum system energy $\tilde{E}_{\min}(\alpha_0)$ for steep angles of attack, parameter combinations above this critical level remain existent. For example, an angle of attack $\alpha_0 = 85^\circ$ (not shown in Fig. 3) necessitates a minimum system energy $\tilde{E}_{\min} = 1.500$, and the lower stability constraint corresponds to a system energy ($\tilde{E}_s^- = 1.497$) below this minimum. Nevertheless, the system energy related to the upper constraint ($\tilde{E}_s^+ = 1.506$) still exceeds the critical level, and, for instance, for a system energy $\tilde{E}_{\min} < \tilde{E}_s = 1.503 < \tilde{E}_s^+$, one easily checks that, besides the steep angle condition(2), with $b - a < 0.06$ the resulting apex return map (26) fulfils Eq. (15) required for the validity of the approximate solution.

As a result of the steep angle $\alpha_0 = 85^\circ$, the return map $y_{i+1}(y_i)$ almost matches the diagonal $y_{i+1} = y_i$, if viewed on the large scale of all possible apex heights, hampering a compact overview of its qualitative behavior. However, to provide such an overview, in Fig. 4, an explicit return map example is shown for the moderate angle of attack $\alpha_0 = 60^\circ$. Here, the system energy $\tilde{E}_s = 1.61$ and, as a result of Eq. (33), the spring stiffness $\tilde{k} = 10.8$ (indicated by the open lines in Fig. 3) are chosen such that the fixed point $y^* = 0.872\ell_0$ (open circle) calculated from Eq. (30) is stable with $\partial_i y^* = 0$. Starting from disturbed apex heights, the system stabilizes within a few steps (as indicated by the arrow traces in the small panel of Fig. 4). Here, the basin of attraction contains all apex heights from the landing height $y_\ell = \ell_0 \sin\alpha_0$ to the second, unstable fixed point (closed circle). As the analysis performed in this section is restricted to local predictions, both the basin and the second fixed point are merely observations from plotting Eq. (26). However, from Fig. 3 it is obtained that, if the system energy is not adequately selected, the fixed point given by Eq. (30) is unstable. Without proof we observed the following behavior: For a system energy leading to $\partial_i y^* < -1$, Eq. (30) still traces the lower fixed point being unstable. For $\partial_i y^* = 1$, both fixed points collapse to a single one, and, if $\partial_i y^* > 1$, Eq. (30) describes the upper, unstable fixed point.

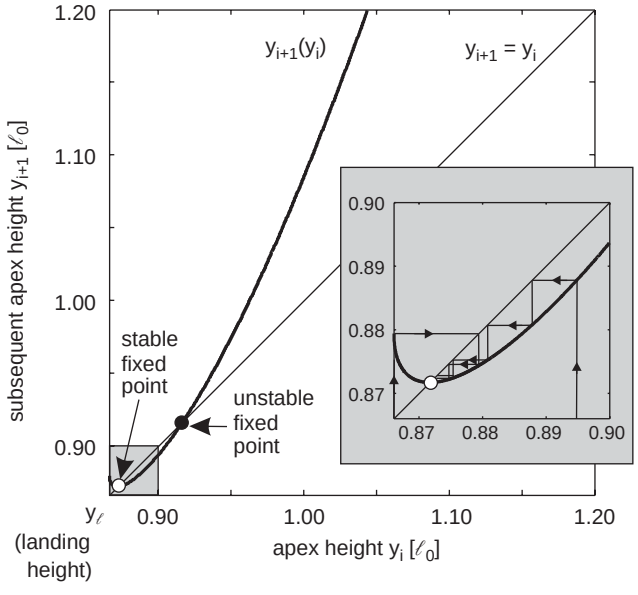

Fig. 4. Stability of spring-mass running. The return map function $y_{i+1}(y_i)$ is shown for the parameter set $\alpha_0 = 60^\circ$, $\tilde{E}_s = 1.61$, and $\tilde{k} = 10.8$, which belongs to the calculated region of parameter combinations producing stable fixed point solutions. As predicted, the return map has a stable fixed point $y_{i+1} = y_i$ attracting neighboring apex states within a few steps (arrow traces in the magnified region). Furthermore, the return map is characterized by an additional, unstable fixed point representing the upper limit of the basin of attraction of the stable one (the lower limit is given by the landing height $y_\ell = \ell_0 \sin\alpha_0$).

4.3.3. k-α_0-relationships for stable running

In the last two sections, we have identified the parameter combinations ($\tilde{k}$, α_0, and $\tilde{E}_s$) required to achieve self-stable running patterns characterized by $a = 0$ (dark area in Fig. 3). Specifically, for steep angles of attack $\alpha_0 \to \frac{\pi}{2}$, stable trajectories are obtained when the system energy $\tilde{E}_s$ is close to the minimum system energy $\tilde{E}_s^{\min}$ (32), i.e. the parametric dependency approaches the minimum stiffness-angle-relation $\tilde{k}^{\min}(\alpha_0)$ (34). In the numerical study (Seyfarth et al., 2002), we empirically found a different estimate for the stiffness-angle-relationship $k(\alpha_0) \approx \frac{1600N}{\ell_0(1-\sin\alpha_0)}$, and the question arises in how far both relationships relate to each other.

Considering that, for $\alpha_0 \to \frac{\pi}{2}$, the minimum system energy $\tilde{E}_s^{\min}$ approaches a value of 1.5, in the numerical study this corresponds to a system energy of $E_s = mg\ell_0\tilde{E}_s \approx 1200\,\mathrm{J}$ ($m = 80\,\mathrm{kg}$, $g = 9.81\,\mathrm{m/s^2}$, and $\ell_0 = 1\,\mathrm{m}$). As the initial apex height was fixed to $y_0 = \ell_0$ therein, this is equivalent to an initial speed of $\dot{x}_0 = \sqrt{\frac{2}{m}(E_s - mg\ell_0)}$ of about 3.3 m/s, which is slightly less than the initial speed the empirical k–α_0-relationship is derived from ($\dot{x}_0 = 5\,\mathrm{m/s}$, Fig. 2A in Seyfarth et al. (2002)). However, the general shape of the stable domain does not change much for initial running velocities below $\dot{x}_0 = 5\,\mathrm{m/s}$ (the domain only narrows, Fig. 2B and C in Seyfarth et al. (2002)) and, hence, from an energetic point of view both relationships should be comparable.

A similar argument holds for the restriction to the special case $a = 0$. As in Seyfarth et al. (2002) running stability is scrutinized for all possible parameter combinations, certainly more than the steady-state solutions belonging to this special case are identified. Actually, the stable domain forms a single volume in the k–α_0–$\dot{x}_0$ space (Geyer, 2001; Seyfarth et al., 2002), which, due to the restriction to the special case $a = 0$, cannot be obtained from Eq. (33). Here, only a surface element of this volume can be derived (dark area in Fig. 3). However, for $\dot{x}_0 \leqslant 5\,\mathrm{m/s}$ the stable parameter domain is rather narrow (for steep angles of attack the angular range is limited to 2°) and, although we do not expect exactly the same result, both the empirical relationship and Eq. (34) should qualitatively be equivalent for $\alpha_0 \to \frac{\pi}{2}$.

Using that for $\alpha_0 \to \frac{\pi}{2}$, $\frac{1}{1-\sin\,\alpha_0} \to \frac{2}{(\frac{\pi}{2}-\alpha_0)^2}$, and taking the body mass used in the numerical study ($m = 80\,\mathrm{kg}$) into account, the empirical k–α_0-relationship can be written as $\tilde{k}_{\alpha_0 \to \frac{\pi}{2}} \approx \frac{4}{(\frac{\pi}{2}-\alpha_0)^2}$. In the same limit Eq. (34) reads $\tilde{k}^{\min}_{\alpha_0 \to \frac{\pi}{2}} = \frac{\pi^2/4}{(\frac{\pi}{2}-\alpha_0)^2}$, which indeed confirms that the qualitative behavior of Eq. (34) is consistent with the empirically found stiffness-angle relation. In addition to this mere comparison, Eq. (33) emphasizes the change of the stiffness-angle relation with increasing system energy, introducing a quality observed but not formulated in the numerical study.

4.4. Quality of approximate solution

Considering the steep angle assumption (2), the valid range of the approximate solution is always bound to a spring stiffness exceeding physiologically reasonable values. For instance, taking the example $\alpha_0 = 85°$ and $\tilde{E}_s = 1.503$ of the last section, the dimensionless stiffness $\tilde{k}(\alpha_0, \tilde{E}_s)$ is $\tilde{k} = 326$. Scaled into absolute values, for a human with a body mass of $m = 80\,\mathrm{kg}$ and a leg length of $\ell_0 = 1\,\mathrm{m}$, the required stiffness $k = \frac{mg}{\ell_0}\tilde{k}$ approaches $260\,\mathrm{kN/m}$. Compared to experiments, where typical stiffness values are in the range of $k = 10 - 50\,\mathrm{kN/m}$ (e.g. Arampatzis et al., 1999), the predicted stiffness is far above the biological range, which, however, is no contradiction since humans do use flatter angles of attack in running (speed dependent, e.g. $\alpha_0 = 60$–$70°$, Farley and Gonzalez (1996)).

At this point, the question arises of how applicable the approximate solution is to biological data, or, more technically spoken, how restrictive are the assumptions made? To gain a quantitative judgement, the quality of the approximation shall be demonstrated by the following example: still considering a human subject with $m = 80\,\mathrm{kg}$ and $\ell_0 = 1\,\mathrm{m}$, the running speed is set to be $\dot{x}_0 = 5\,\mathrm{m/s}$ at the apex $y_0 = \ell_0$, and a leg stiffness $k = 11\,\mathrm{kN/m}$ and an angle of attack $\alpha_0 = 60°$ are assumed. The contact phase of the resulting steady-state motion is characterized by a maximum spring compression of 20%, which corresponds to a relative spring amplitude $\rho = -0.2$. At this configuration, the accuracy (i.e. the maximum error) of the analytically predicted center of mass trajectory ((21) and (22)) is better than 1% in spring compression and 0.6° for the angle swept during stance ($|\Delta\varphi| = 60°$) compared to the numerical counterpart.

This indicates that, even for configurations with reasonable angles of attack, the approximate solution well describes the dynamics of the stance phase. However, it cannot be concluded with such a single example whether the quality of the solution satisfies the demands of a specific application. To illustrate its predictive power in the context of self-stability, in Fig. 5 the parameter combinations leading to self-stable movement trajectories (Fig. 5A–C) are compared to numerical results (Fig. 5D–F, after Seyfarth et al. (2002)) throughout the parameter space. Although, for the stability of steady-state trajectories, it would suffice to compare the analytically predicted with the numerically calculated apex return maps for each single parameter combination, in Fig. 5 the investigation of the number of successful steps is adopted from Seyfarth et al. (2002). This not only allows a direct comparison to the numerical and experimental results presented in Seyfarth et al. (2002), but, starting from disturbed apex conditions, also scrutinizes the performance of the approximate apex return map (26) if consecutively applied, hereby addressing the influence of the arbitrary energy correction following each stance phase (Section 4.2) on the quality of the approximate solution. For angles of attack $\alpha_0 \geqslant 60°$, the predicted region matches the simulation results surprisingly well. This holds not only for the general shape, but also for the subtle details (e.g. the sharp edges in the stability region close to the level of $\dot{x}_0 = 5\,\mathrm{m/s}$ in Fig. 5B and C, E and F, respectively). Again, a quantitative comparison shall be provided: For $\alpha_0 = 60°$, the range of spring stiffness resulting in stable running narrows from $2\,\mathrm{kN/m}$ (10.5–12.5 kN/m, Fig. 5D) to $1.6\,\mathrm{kN/m}$ (10.6–12.2 kN/m,Fig. 5A). Complementary, for a given spring stiffness of $k = 11\,\mathrm{kN/m}$, the angle of attack range narrows from 2.7° (58.0 − 60.7°) to 1.7° (58.6–60.3°).

5. Discussion

In this study, we addressed the stability of spring-mass running within a theoretical framework. We derived an analytical solution for the stance phase dynamics assuming steep spring angles and small spring compressions, and investigated the return map of the

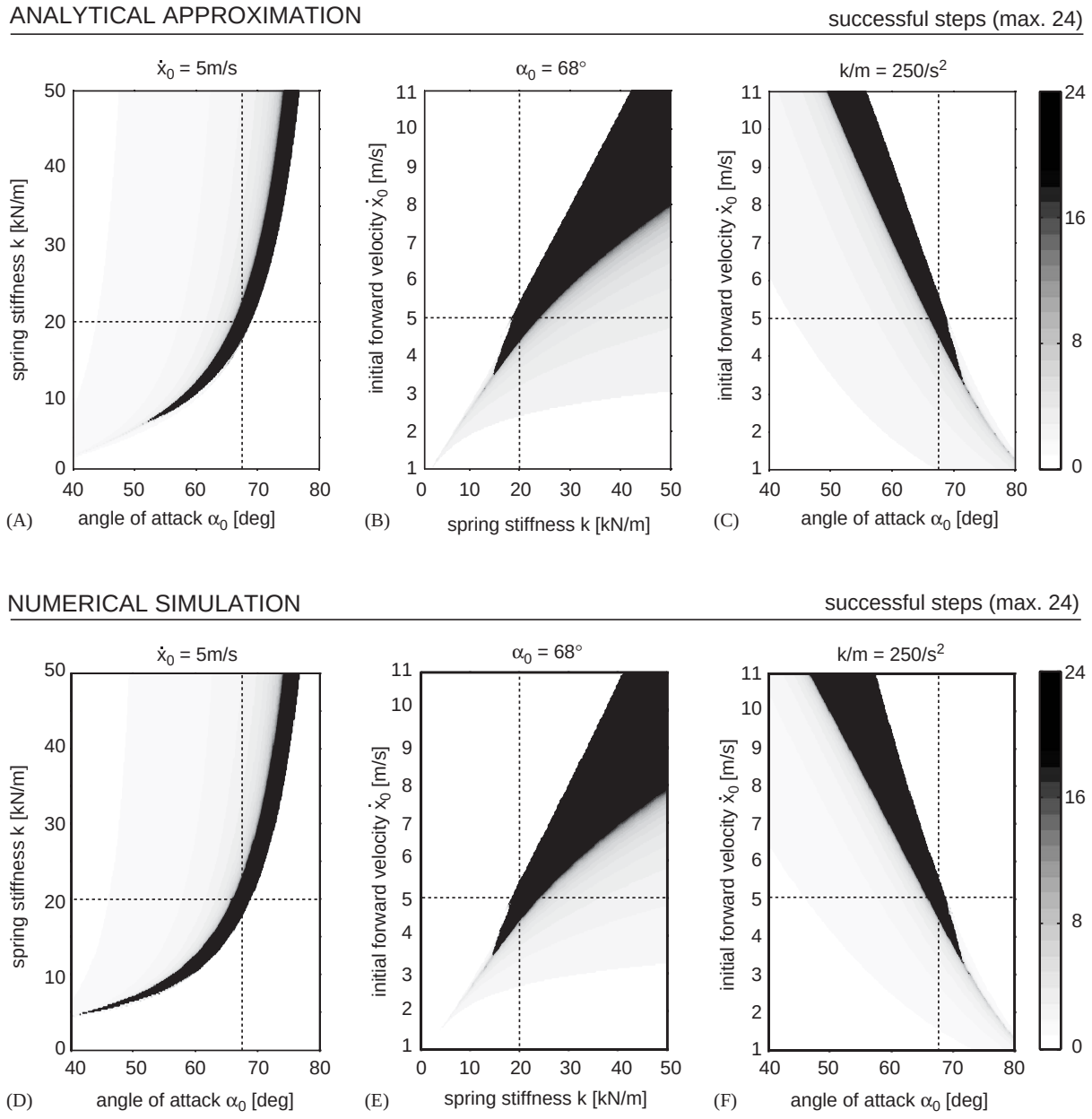

Fig. 5. Comparison of the stability region for spring-mass running predicted by the analytical approximation (A–C) with the results from a previous simulation study (Seyfarth et al., 2002) (D–F). Starting from the initial condition $y_0 = \ell_0$ and $\dot{x}_0$, the number of successful steps is predicted by iteratively applying the return map function (26) (A–C), or obtained through numerical integration of the spring-mass system (D–F). The movement is interrupted if (i) the vertical or horizontal take-off velocity becomes negative, or (ii) the number of successful steps exceeds 24 (scale on the right). In each subplot (A–C, or D–F, respectively), one of three parameters $(k, \alpha_0, \dot{x}_0)$ is held constant. *Additional parameters:* $m = 80\,\mathrm{kg}$, $g = 9.81\,\mathrm{m/s^2}$, $\ell_0 = 1\,\mathrm{m}$, and $E_s = \frac{m}{2}\dot{x}_0^2 + mg\ell_0$.

apex height. The analysis confirms the previously identified self-stabilization of spring-mass running. Moreover, the stability prediction surprisingly well matches the numerical results throughout the parameter space (leg stiffness k, angle of attack $\alpha \geqslant 60°$, and system energy E_s or, adequately, initial forward speed $\dot{x}_0$), suggesting that, within this range, the approximate solution sufficiently describes the dynamics of the center of mass during the stance phase of spring-mass running. The solution is not restricted to the parameter setups used in this study, but also holds in dynamically similar situations (Blickhan, 1989).

5.1. Closed form representations of the stance phase dynamics

As mentioned in the introduction, the stance phase dynamics of the spring-mass model are non-integrable

(Whittacker, 1904) and, thus, approximate solutions are in demand when seeking parametric insights into the properties of the system. A common approach to this issue is to simply ignore the gravitational force. The resulting central force problem allows a closed form solution in the formal mathematical sense, which, however, involves elliptic integrals (Schmitt and Holmes, 2000) and, therefore, lacks a representation in elementary functions hampering the desired parametric insight. At this point, one either proceeds by resuming to numerical studies (e.g. Ghigliazza et al., 2003), or further simplifications are introduced. For instance, in Schwind and Koditschek (2000) the mean value theorem is applied to circumvent elliptic integrals yielding a good approximation of the modified system dynamics in stance, especially, when the spring compression is close to its maximum.

However, in these studies it is also demonstrated that the effects of gravity can hardly be neglected in general locomotion (Schwind and Koditschek, 2000) or when using physiologically motivated model parameters (Geyer, 2001). The resulting approximate solutions clearly deviate from numerical calculations for the spring-mass model incorporating gravity (e.g. in Schwind and Koditschek (2000) mean errors as high as 20% for the radial velocity at take-off are observed). Although these solutions may be used for qualitative assessments (Ghigliazza et al., 2003), any quantitative result seems highly questionable. Bearing in mind that the spring-mass model is employed to devise general control schemes for running machines (Raibert, 1986; Saranli and Koditschek, 2003) and to investigate animal and human locomotion (He et al., 1991; Farley et al., 1991, 1993; Seyfarth et al., 2001), this leaves a rather unsatisfactory state.

To surmount the discrepancy, in Schwind and Koditschek (2000) a general approach similar to Picard iterations is introduced that iteratively fits the solution without gravity in stance to the complete system. The algorithm does not depend on the particular spring law, and changes of angular momentum as observed in the complete spring-mass system are taken into account. Again, this approach best approximates the solution for the instant of maximum spring compression, although it seems that, with an increasing number of iterations, the result for the subsequent apex condition also improves (in Schwind and Koditschek (2000) the 'bottom-to-apex map' from maximum spring compression to apex position is investigated). The authors report a reduction of the largest mean errors from 20% for the zeroth iterate (solution without gravity) to 7% for the first iterate and to 3.5% for the second iterate. Yet with increasing number of iterates, the algebraic tractability of the approximate solution decreases. However, it should be noted that, although most of the model parameters in Schwind and Koditschek (2000) are human-like, a body mass of $m = 1\,\mathrm{kg}$ is used, and the correct assessment of accuracy in the physiological parameter domain requires re-investigation for this approximation.

Similar to existing approaches, the approximate solution derived in this study is based on a simplification of the stance-phase dynamics to a central force problem rendering the planar spring-mass model integrable. But instead of ignoring gravity, the gravitational force vector is realigned from the vertical to the spring axis. This approach is motivated by the assumption of steep spring angles during stance. By introducing the further assumption of small spring amplitudes, a Taylor series expansion allows to rewrite the resulting differential equation for the radial motion into an integral equation of familiar type ($\int \frac{\mathrm{d}x}{ax^2+bx+c}$). Although the dynamics of the central force system could have been obtained by consequently solving elliptic integrals, this approach avoids the difficult quadratures that typically remain even when gravity is ignored (e.g. Schmitt and Holmes, 2000; Ghigliazza et al., 2003). Hence, the radial and angular motions can be extracted in terms of elementary functions. But, more importantly, the approximation error introduced by using the Taylor series expansions in part compensates for the error made by converting the planar spring-mass model into a central force system (see appendix). In consequence, the exemplified approach combines a comparatively simple solution with surprising accuracy well extending into the physiologically motivated parameter domain (compare Fig. 5). Although a Hooke's law spring has been considered in this study, the applied ideas might be transferable to other spring potentials as well.

However, it should not be overlooked that, for any approximation based on the central force system approach during stance, the conservation of system energy is inherently violated for asymmetric contact phases (take-off height unequal to touch-down height). A pragmatic solution to this is to simply restore the preset system energy at take-off, for instance, by artificially manipulating the vertical and/or horizontal take-off velocity (Saranli et al., 1998; Ghigliazza et al., 2003). We resolved this discrepancy in the same manner (by forcing E_s to be constant, the horizontal velocity is automatically adapted in the next flight phase), but would like to emphasize that, in a formal mathematical sense, there is not yet any justification of such a method guaranteeing the exact same qualitative behavior of approximate solution and complete spring-mass model. The only confidence we can reach is that (i) steady-state solutions are characterized by symmetric contact phases, where the conservation of system energy equally holds for central force approximations, and (ii) in a small neighborhood of such an equilibrium state the change in system energy seems negligible compared to the system energy itself.

Without doubt, if flat spring angles are considered, the quality of the solution decreases, and further approximation refinements are required incorporating the effects of the accurate alignment of the gravitational force during stance. For instance, it could be tested whether the derived approximate solution would provide a better zeroth iterate for the algorithm suggested in Schwind and Koditschek (2000). As gravity has been taken into account except for the exact alignment with the vertical axis, the iterative solution might converge faster to a result within a certain, small error tolerance compared to numerical calculations. On the other hand, since the misalignment of gravity only causes rather small changes for steep spring angles, classical perturbation theory might be applicable, possibly yielding better results for a larger angular range.

5.2. Self-stability and control of spring-mass running

Before investigated in sagittal plane running, the self-stabilizing property of the spring-mass system could be demonstrated when modeling the alternating tripod of six-legged insects in the horizontal plane (Schmitt and Holmes, 2000). As gravity is not interfering in this case, the authors benefitted from the mean value approximation of Schwind and Koditschek (2000) (compare last section) replacing the numerical computation of the angle swept during stance with an analytical expression.

In a simulation study, it could later be shown that, by simply resetting the spring orientation (angle of attack) during the flight phase, the spring-mass model can also exhibit self-stable behavior in sagittal plane running in the presence of gravity (Seyfarth et al., 2002). By mapping the model behavior throughout the parameter space (spring stiffness, angle of attack, and initial running velocity), the required parameter combinations for self-stable spring-mass running were compared with data from human running. It was found that biological systems seem well to adapt to the predicted parameter domain. Subsequently, in Ghigliazza et al. (2003) this model was investigated within a more theoretical framework. Apart from the angle swept during stance, which was still calculated by numerical integration, the authors derived an explicit expression for the return map of spring-mass running by neglecting gravity during stance. By not aiming at quantitative comparisons with specific animals or machines, they could (i) clarify some of the general observations made in Seyfarth et al. (2002) (e.g. minimum running speed), and (ii) illustrate key behaviors of the derived return map (e.g. bifurcation and period doubling).

In contrast to other approaches, the stability analysis performed in this study is based on the apex return map derived from an approximate solution of the stance phase dynamics including gravity. For a special case ($a = 0$), we could show the existence of stable fixed point solutions in spring-mass running without having to recourse numerical integrations. We hereby confirmed the qualitative behavior of an empirically found parametric dependency for stable running between spring stiffness and angle of attack, and extended it by the system energy. Furthermore, by comparing the predicted parameter combinations for stable running with numerical results, we observed a quantitative agreement far beyond the valid range of the approximate solution, suggesting that, whether in biomechanics or robotics, if the stability of bouncing gaits is of concern, the presented solution may well serve as an analysis tool.

For instance, it could be investigated to what extent the stability of movement trajectories can be manipulated when incorporating leg swing policies other than the fixed leg orientation (Seyfarth et al., 2002; Ghigliazza et al., 2003) during flight. In a recent investigation (Altendorfer et al., 2003), a necessary condition for asymptotic stability could be derived when incorporating specific leg recirculation schemes relevant for the robot RHex (Saranli et al., 2001). Based on the factorization of return maps, in this special application, the condition was formulated as an exact algebraic expression without having to resort to the actual stance-phase dynamics.

However, no information about the system's behavior could be obtained from this condition when applied to a retracting swing leg policy. Here, recent simulation studies (Seyfarth and Geyer, 2002; Seyfarth et al., 2003) suggest that the stability of running can largely be enhanced. In particular, it could be demonstrated that a simple feedforward kinematic leg-angle program $\alpha(t - t_{apex})$ during flight can enforce the movement trajectory of spring-mass running to a 'dead beat' (Saranli et al., 1998) behavior: independent of the actual apex height y_i, the next apex height y_{i+1} resumes to a preset steady-state height $y_{control}$, guaranteeing 'maximum' stability $y_{i+1}(y_i) = y_{control}$. Of course, this can only be achieved if a critical apex height $y_{\min} = \ell_0 \sin \alpha_{apex}$ is exceeded. Different initial apex heights can also be considered as alternating ground levels with respect to one absolute apex height and, thus, the kinematic leg program allows to choose a high level of running safety ($y_{control}$ far above $y_{\min}$, bouncy gait as observed in kangaroos). As the model is conservative, such a 'secure', bouncy movement would exhaust the energy available for forward locomotion, which might not be required in flat, predictable terrain. Accordingly, by selecting an apex height $y_{control}$ close to the minimum height $y_{\min}$, the kinematic leg program allows to maximize the energy efficiency (the share of system energy spent for forward locomotion). Such a flexibility, strongly reminiscent of animal behavior, could largely enhance the repertoire of movement patterns available to legged machines.

Despite these progresses, whether the observed self-stabilizing behavior has been ascribed to 'angular

momentum trading' (Schmitt and Holmes, 2000) or 'enforced energy distribution among the systems degrees of freedom' (Geyer et al., 2002), we still lack a comprehensive understanding of the key features responsible for its emergence. What properties of the system dynamics during stance allow a proper interaction with the gravitational force field during flight yielding self-stability in the regime of intermittent contacts? And, further on, in how far can we manipulate these properties? Intensifying theoretical approaches seems desirable at this point since they might not only support suggested control strategies, but could also disclose further and maybe not obvious alternatives.

5.3. Conclusion

Considering this lack of knowledge and comparing the ease and maneuverability distinguishing animal and human locomotion with the skills of legged machines, the investigation of gait stabilization in biological systems seems to be a substantial research direction. Here, the planar spring-mass model served as an efficient analysis tool in the past. Benefitting from its parametric simplicity, its stabilizing behavior could well be investigated by purely numerical means (dependence on three parameter groups only). Yet the situation rapidly changes if more complex models of locomotion are addressed, for instance, when incorporating leg recirculation strategies during flight and/or investigating the stability of locomotion in three dimensions. At this point, numerical approaches become more difficult and tractable analytical descriptions more important. In the simplest case, approximate solutions could substitute the numerical calculation of the stance phase dynamics significantly reducing the computational effort. In the best case, they could provide the parametric insight themselves (e.g. as exemplified by Eq. (33)). In that sense, the relevance of the presented approximate solution may be seen in its simplicity and predictive power within the physiological parameter domain, which allows to experimentally validate further control strategies of biological systems likely to be disclosed in more complex models of legged locomotion than the simple planar spring-mass system.

Acknowledgements

We would like to thank Prof. Philip Holmes and the anonymous reviewers for a number of helpful comments and suggestions on the manuscript. This research was supported by a grant of the German Academic Exchange Service (DAAD) within the 'Hochschulsonderprogramm III von Bund und Länder' to HG and an Emmy-Noether grant (SE1042/1-4) of the German Science Foundation (DFG) to AS.

Appendix A. Mixed accuracy approximation of $\frac{1}{(1+\rho)^2}$

The central force approximation of the stance phase dynamics captures an important feature of the planar spring-mass model: the presence of the centrifugal force $\mathbf{F}_c = mr\dot{\varphi}^2\mathbf{e}_r$ accelerating the compression-decompression cycle of the spring. In consequence, the oscillation frequency $\hat{\omega}_0$ of the planar system is increased when compared to the frequency $\omega_0 = \sqrt{k/m}$ of the corresponding one-dimensional system (vertical spring-mass model). To account for such an increase, the Taylor expansion of $\frac{1}{(1+\rho)^2}$ must be performed to at least second order in ρ (9). Otherwise, $\hat{\omega}_0$ would equal ω_0 and the radial motion (12) or (21) would represent the motion of a vertical spring-mass system hardly resembling the planar dynamics.

On the other hand, the central force approximation also introduces a substantial drawback: the conservation of initial angular momentum $P_{TD} = m\ell_0^2\dot{\varphi}_{TD}$ throughout stance. Although the net change in angular momentum is zero for symmetric (time-reflection symmetry about midstance $t_{mid} = t_c/2$) contacts of the planar spring-mass system, the mean angular momentum

$$\bar{P} = \frac{1}{t_c}\int_0^{t_c} P(t)\,\mathrm{d}t \tag{A.1}$$

changes ($\bar{P} \neq P_{TD}$). Expressing $P(t)$ by the initial value and the rate of change $P(t) = P_{TD} + \int_0^t \dot{P}(t')\,\mathrm{d}t'$, and using $\dot{P}(t') = -mgr(t')\cos\varphi(t') = -mgx(t')$ for the planar spring-mass system, we obtain

$$\begin{aligned}\bar{P} &= P_{TD} - \frac{mg}{t_c}\int_0^{t_c}\int_0^{t} x(t')\,\mathrm{d}t'\,\mathrm{d}t \\ &= P_{TD} - \frac{mg}{t_c}\left[\int_0^{t_{mid}}\int_0^{t} x(t')\,\mathrm{d}t'\,\mathrm{d}t \right. \\ &\quad \left. + \int_{t_{mid}}^{t_c}\int_0^{t_{mid}} x(t')\,\mathrm{d}t' + \int_{t_{mid}}^{t_c}\int_{t_{mid}}^{t} x(t')\,\mathrm{d}t'\,\mathrm{d}t\right].\end{aligned} \tag{A.2}$$

Using that, for symmetric contacts, at midstance the horizontal position x switches from negative-to-positive values, Eq. (A.2) can be written as

$$\begin{aligned}\bar{P} &= P_{TD} + \frac{mg}{t_c}\left[\int_0^{t_{mid}}\int_0^{t} |x(t')|\,\mathrm{d}t'\,\mathrm{d}t \right. \\ &\quad + \int_{t_{mid}}^{t_c}\int_0^{t_{mid}} |x(t')|\,\mathrm{d}t'\,\mathrm{d}t \\ &\quad \left. - \int_{t_{mid}}^{t_c}\int_{t_{mid}}^{t} |x(t')|\,\mathrm{d}t'\,\mathrm{d}t\right].\end{aligned} \tag{A.3}$$

The time reflection symmetry about midstance yields $\int_{t_{mid}}^{t_c} = \int_0^{t_{mid}}$, and (A.3) simplifies to

$$\begin{aligned}\bar{P} &= P_{TD} + \frac{mg}{t_c}\int_{t_{mid}}^{t_c}\int_0^{t_{mid}} |x(t')|\,\mathrm{d}t'\,\mathrm{d}t \\ &= P_{TD} + \frac{mg}{2}\int_0^{t_{mid}} |x(t')|\,\mathrm{d}t'.\end{aligned} \tag{A.4}$$

The mean angular momentum is increased compared to the initial value, which, however, means that the amount of mean angular momentum decreases $|\bar{P}|<|P_{TD}|$ since the initial value P_{TD} is negative (according to the definition of the coordinate system in Fig. 1 the angular velocity $\dot{\varphi}$ is defined negative for forward motion).

The miscalculation of angular momentum in the central force approach ($P \equiv P_{TD}$) has a more profound effect on the angular motion ($P \sim \dot{\varphi}$) than on the radial ($P \sim r^2$). Considering that, due to the alignment of the gravitational force with the radial axis ($-mg \sin \varphi \to -mg$ in (3)), the spring compression is increased, this leads to a clear overestimation of the angular velocity.

Here, an approximation of the central force system dynamics with an error decreasing this inherent overestimation may result in a better performance when compared to the actual spring-mass dynamics. Considering $\frac{1}{(1+\rho)^2}$, the Taylor expansion to the nth order about $\rho = 0$ is given by

$$\left.\frac{1}{(1+\rho)^2}\right|_{\rho=0} = \sum_{i=0}^{n} (-1)^i (i+1)\rho^i. \tag{A.5}$$

Since $\rho \leqslant 0$ during contact, this simplifies to

$$\begin{aligned}\left.\frac{1}{(1+\rho)^2}\right|_{\rho=-0} &= \sum_{i=0}^{n} (i+1)|\rho|^i \\ &= 1 + 2|\rho| + 3|\rho|^2 + \cdots + (n+1)|\rho|^n\end{aligned} \tag{A.6}$$

showing that the approximation of angular velocity $\dot{\varphi} = \frac{\omega}{(1+\rho)^2}$ increases with each expansion term. Hence, it might be advantageous to cancel this expansion earlier than second order. In fact, it turns out it is. Comparing different order (zeroth-to-second) approximations of $\frac{1}{(1+\rho)^2}$ for $\dot{\varphi}$ with numerical computations of the actual spring-mass dynamics, the first-order approximation performs best.

References

Alexander, R.M., 1989. Optimization and gaits in the locomotion of vertebrates. Physiol. Rev. 69, 1199–1227.

Altendorfer, R., Koditschek, D.E., Holmes, P., 2003. Towards a factored analysis of legged locomotion models. In: Proceedings of the International Conference on Robotics and Automation. Taipei, Taiwan, pp. 37–44.

Arampatzis, A., Brüggemann, G., Metzler, V., 1999. The effect of speed on leg stiffness and joint kinetics in human running. J. Biomech. 32, 1349–1353.

Blickhan, R., 1989. The spring-mass model for running and hopping. J. Biomech. 22, 1217–1227.

Blickhan, R., Full, R.J., 1993. Similarity in multilegged locomotion: bouncing like a monopode. J. Comp. Physiol. 173, 509–517.

Coleman, M.J., Holmes, P., 1999. Motions and stability of a piecewise holonomic system: the discrete chaplygin sleigh. Regul. Chaot. Dynamics 4 (2), 1–23.

Coleman, M.J., Chatterjee, A., Ruina, A., 1997. Motions of a rimless spoked wheel: a simple three-dimensional system with impacts. Dynamics Stability Systems 12, 139–159.

Farley, C.T., Gonzalez, O., 1996. Leg stiffness and stride frequency in human running. J. Biomech. 29 (2), 181–186.

Farley, C.T., Blickhan, R., Saito, J., Taylor, C.R., 1991. Hopping frequency in humans: A test of how springs set stride frequency in bouncing gaits. J. Appl. Physiol. 71 (6), 2127–2132.

Farley, C.T., Glasheen, J., McMahon, T.A., 1993. Running springs: speed and animal size. J. Exp. Biol. 185, 71–86.

Geyer, H., 2001. Movement criterion of fast locomotion: mathematical analysis and neuro-biomechanical interpretation with functional muscle reflexes. Diploma Thesis.

Geyer, H., Blickhan, R., Seyfarth, A., 2002. Natural dynamics of spring-like running—emergence of selfstability. In: Proceedings of the Fifth International Conference on Climbing and Walking Robots. Professional Engineering Publishing Limited, pp. 87–92.

Ghigliazza, R.M., Altendorfer, R., Holmes, P., Koditschek, D.E., 2003. A simply stabilized running model. SIAM J. Appl. Dynamical Systems 2 (2), 187–218.

He, J.P., Kram, R., McMahon, T.A., 1991. Mechanics of running under simulated low gravity. J. Appl. Physiol. 71 (3), 863–870.

McMahon, T.A., Cheng, G.C., 1990. The mechanism of running: how does stiffness couple with speed? J. Biomech. 23, 65–78.

Raibert, M.H., 1986. Legged Robots that Balance. MIT Press, Cambridge.

Ruina, A., 1998. Non-holonomic stability aspects of piecewise holonomic systems. Rep. Math. Phys. 42 (1/2), 91–100.

Saranli, U., Koditschek, D.E., 2003. Template based control of hexapedal running. In: Proceedings of the IEEE International Conference on Robotics and Automation, Taipei, Taiwan, pp. 1374–1379.

Saranli, U., Schwind, W.J., Koditschek, D.E., 1998. Towards the control of a multi-jointed, monoped runner, leuven, Belgium. In: Proceedings of the IEEE International Conference on Robotics and Automation, pp. 2676–2682.

Saranli, U., Buehler, M., Koditschek, D.E., 2001. Rhex: A simple and highly mobile hexapod robot. Int. J. Robotics Res. 20 (7), 616–631.

Schmitt, J., Holmes, P., 2000. Mechanical models for insect locomotion: dynamics and stability in the horizontal plane I. Theory. Biol. Cybern. 83, 501–515.

Schwind, W.J., Koditschek, D.E., 2000. Approximating the stance map of a 2-DOF monoped runner. J. Nonlinear Sci. 10, 533–568.

Seyfarth, A., Geyer, H., 2002. Natural control of spring-like running—optimized self-stabilization. In: Proceedings of the Fifth International Conference on Climbing and Walking Robots. Professional Engineering Publishing Limited, pp. 81–85.

Seyfarth, A., Apel, T., Geyer, H., Blickhan, R., 2001. Limits of elastic leg operation. In: Blickhan, R. (Ed.), Motion Systems 2001. Shaker Verlag, Aachen, pp. 102–107.

Seyfarth, A., Geyer, H., Günther, M., Blickhan, R., 2002. A movement criterion for running. J. Biomech. 35, 649–655.

Seyfarth, A., Geyer, H., Herr, H.M., 2003. Swing-leg retraction: a simple control model for stable running. J. Exp. Biol. 206, 2547–2555.

Whittacker, E.T., 1904. A treatise on the analytical dynamics of particles and rigid bodies, Fourth ed. Cambridge University Press, New York.

Wickler, S.J., Hoyt, D.F., Cogger, E.A., Hall, K.M., 2001. Effect of load on preferred speed and cost of transport. J. Appl. Physiol. 90, 1548–1551.